Model for current drive stabilization of neoclassical tearing modes

Jennifer Woodby, Eugenio Schuster, Glenn Bateman, and Arnold H. Kritz
Lehigh University, Bethlehem, Pennsylvania 18015, USA

(Received 2 July 2008; accepted 6 August 2008; published online 9 September 2008)

A model derivation is presented for the effect of current drive on the saturated width of magnetic islands driven by the neoclassical tearing mode instability in axisymmetric plasmas. The derivation is carried out for continuous current drive as well as for modulated current that is driven at the same angle as the island O-point. The results of the derivation are implemented in a revision of the ISLAND module to compute saturated magnetic island widths. It is found that the greatest stabilizing effect of both modulated and continuous current drive on the island width is achieved when current is driven at the island center. In addition, narrow current drive is more effective at stabilizing the magnetic islands than wide current drive, for which more current falls outside the island. When modulated and continuous current drives are compared for equal total driven current, the modulated current is shown to be more effective, particularly as the offset from the island center increases. © *2008 American Institute of Physics*. [DOI: 10.1063/1.2976366]

I. INTRODUCTION

The neoclassical tearing mode (NTM) instability produces magnetic islands in tokamak plasmas that can degrade confinement and lead to plasma disruptions. The central physical process that is responsible for NTMs is the bootstrap current density driven by the plasma pressure gradient outside of magnetic islands. Inside magnetic islands, the pressure profile is locally flattened, and the pressure gradient is nearly absent. The lack of bootstrap current within each island produces a helical perturbation in the total current density, which enhances the NTM instability and increases the width of the resulting magnetic island. NTMs can be stabilized by driving current locally within each magnetic island in order to replace the missing bootstrap current density. A model for the stabilization of NTMs by localized current drive is presented in this paper.

Magnetic islands produced by NTMs have been observed in tokamak experiments.[1–7] As tokamaks operate with higher pressure and longer pulse lengths, NTMs become more deleterious. The most damaging magnetic islands are those with low poloidal and toroidal mode numbers, e.g., $m/n=2/1$, $3/2$, where m is the poloidal mode number (the short way around) and n is the toroidal mode number (the long way around the tokamak). Since NTMs are stable for sufficiently small magnetic island widths, a "seed" perturbation is required in order to start NTM island growth. Hence, in general, NTMs are linearly stable and nonlinearly unstable. For stabilization, it is sufficient to shrink the islands to a critical width below which they continue to shrink on their own.[8]

In recent years, progress has been made in the physics understanding[4] and the control of NTMs.[9] Currently, strategies to avoid and suppress NTMs in order to maintain stability include: (1) reducing or eliminating noise from other instabilities in order to keep the NTM seed islands sufficiently small; (2) using helical fields from other, benign, modes or externally applied fields to inhibit the perturbed bootstrap currents of modes of concern; or (3) applying radio frequency (rf) power current drive [e.g., electron cyclotron current drive (ECCD), Ref. 10] parallel to the equilibrium plasma current at mode rational surfaces in order to increase the linear stability and replace the "missing" bootstrap current within magnetic islands. The last of these stabilization methods—current drive within each magnetic island—is the focus of this paper.

The theory of tearing mode stabilization in toroidal plasmas by rf driven currents that are modulated in phase with the island rotation has been previously studied in Ref. 11. In that paper, transient effects such as finite time response of the driven current are considered, and a dynamical model is developed. In this paper, only the steady state solution is considered for continuous or for modulated current drive. Here, the effect of localized current drive is modeled and implemented in the revised ISLAND module[12,13] to compute the saturated magnetic island widths. The ISLAND module in the National Transport Code Collaboration Module Library (http://w3.pppl.gov/NTCC) contains an implementation of a quasilinear model to compute magnetic island widths of saturated neoclassical tearing modes. The NTCC ISLAND module is intended to be used for axisymmetric toroidal plasmas with arbitrary aspect ratio, cross-sectional shape, and plasma β. An adaptive ordinary differential equation (ODE) solver is used in a shooting method to integrate a coupled system of ODEs for harmonics of the magnetic perturbation, which are derived from the three-dimensional scalar plasma pressure force balance equations. An additional term representing the effects of localized current drive in the coupled system of ODEs is included in the revised ISLAND module that is employed in this paper.

In this paper, the effect of localized current drive on the saturated widths of magnetic islands is investigated. In Sec. II, the procedure for determining saturated magnetic island widths without current drive is outlined. In Sec. III, a Gaussian current drive term is introduced, and the derivation of Sec. II is repeated for the resulting total current profile including the current drive. In Sec. IV, the mathematical dif-

ferences between modulated current driven at the island O-point and continuously driven current are presented. In Sec. V, the normalization procedure for the differential flux surface areas is explained. Section VI contains the computation of total driven current in Amperes. Section VII shows the results of implementation of localized current drive in the revised ISLAND module for both modulated and continuous current drive profiles. In Sec. VIII conclusions are presented.

II. SATURATED ISLAND WIDTHS WITHOUT CURRENT DRIVE

By following the derivation presented in Ref. 14, a system of ordinary differential equations can be derived for the solution of the three-dimensional plasma equilibrium force-balance equations

$$\mathbf{J}\times\mathbf{B}=\nabla p, \tag{1}$$

$$\nabla\times\mathbf{B}=\mu_0\mathbf{J}, \tag{2}$$

$$\nabla\cdot\mathbf{B}=0, \tag{3}$$

where $\mathbf{J}$ is the current density, $\mathbf{B}$ is the magnetic field, p is the scalar pressure, and μ_0 is the permeability of free space. These equations are expressed in Hamada-type coordinates (V,θ,ζ), where V is a flux surface label, θ is a poloidal anglelike variable, and ζ is a toroidal anglelike variable.[14] A small perturbation about an axisymmetric equilibrium field is applied, $\mathbf{B}=\mathbf{B}^0+\mathbf{B}^1$, where superscript "0" denotes the unperturbed axisymmetric field and superscript "1" represents the first order perturbation. There are corresponding perturbations in the current density $\mathbf{J}$ and the plasma pressure p. Equations (1)–(3) are expressed in terms of a combination of contravariant and covariant components. All perturbed variables X^1 are written as a series of Fourier harmonics in θ and ζ with the form,

$$X^1(V,\theta,\zeta)=\sum_{m,n}X^1_{mn}(V)\exp[i(m\theta-n\zeta)]. \tag{4}$$

The divergence-free property of the perturbed magnetic field, $\nabla\cdot\mathbf{B}^1=0$, can then be written in terms of the contravariant components of $\mathbf{B}^1$ as[14]

$$\frac{d}{dV}(-i\mathcal{J}B^{1V}_{mn})=n\mathcal{J}B^{1\zeta}_{mn}-m\mathcal{J}B^{1\theta}_{mn}, \tag{5}$$

where $\mathcal{J}=(\nabla V\cdot\nabla\theta\times\nabla\zeta)^{-1}$ is the Jacobian of the axisymmetric coordinates, and the superscripts V, ζ, θ indicate contravariance. The other perturbation equations can be combined to yield

$$(nB^{0\zeta}-mB^{0\theta})\left(\frac{d}{dV}B^1_{\theta mn}-imB^1_{Vmn}\right)$$
$$=\mu_0(nJ^{0\zeta}-mJ^{0\theta})\mathcal{J}B^{1\zeta}_{mn}-i\mathcal{J}B^{1V}_{mn}B^{0\zeta}\frac{d}{dV}\frac{\mu_0J^{0\zeta}}{B^{0\zeta}}$$
$$+m\mu_0p^1_{mn}\frac{1}{B^{0\zeta}}\frac{d}{dV}B^{0\zeta}, \tag{6}$$

where the subscripts V and θ indicate covariant components of the perturbed field.

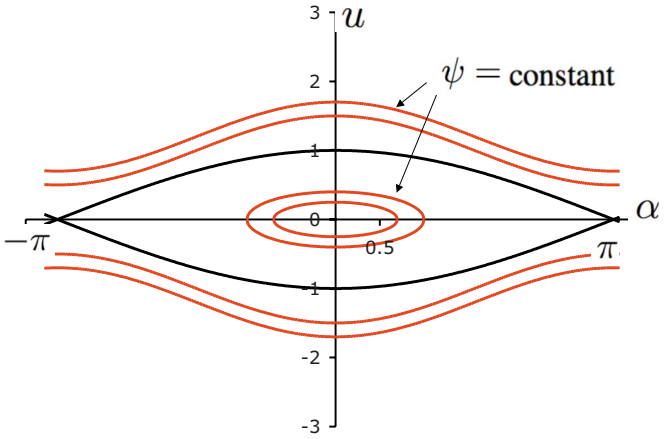

FIG. 1. (Color online) Surfaces of constant magnetic flux ψ.

Equations (5) and (6) yield a coupled pair of ordinary differential equations for each helical harmonic of the variables $[-i\mathcal{J}B^{1V}_{mn},B^1_{\theta mn}]$. Additional algebraic equations can be derived to provide a closed set of equations. A flat spot in the normalized current density $\mu_0J^{0\zeta}/B^{0\zeta}$ and the plasma pressure p is produced by the presence of a magnetic island at a mode rational surface where $nB^{0\zeta}-mB^{0\theta}=0$. These local flat spots prevent the differential equations from being singular at mode rational surfaces. An iterative algorithm is used to determine the saturated tearing mode island widths as eigenvalues of the differential boundary value equations. This algorithm has been implemented in the NTCC ISLAND module.[14] In this paper, the normalized current density term $\mu_0J^{0\zeta}/B^{0\zeta}$ in Eq. (6) is modified in order to take into account the effects of the applied rf current drive.

The local flattening effect of each magnetic island on the normalized current density profile is outlined here. A similar approach applies to the effect of each magnetic island on the pressure profile. Consider a stream function ψ that is uniform along magnetic field lines, $\mathbf{B}\cdot\nabla\psi=0$. The Taylor series expansion of ψ in the neighborhood of a magnetic island has the form

$$\psi=\psi^0_{mn}-2\psi^1_{mn}u^2+\cdots+\psi^1_{mn}\cos\alpha, \tag{7}$$

where $\alpha\equiv m\theta-n\zeta$ is a helical angle coordinate and $u=(V-V_{mn})/H_{mn}$ is the normalized minor radius around the location of the mode rational surface V_{mn}, where $q\equiv B_{0\zeta}/B_{0\theta}=m/n$, and where H_{mn} is magnetic island half-width given by[14,15]

$$H_{mn}=2\sqrt{\left[\frac{-iB_{1V}mn}{nB_{0\theta}(dq/dV)}\right]_{V=V_{mn}}}. \tag{8}$$

Surfaces of constant ψ are illustrated in Fig. 1. Equation (7) can be used to define a mapping from $u'(\alpha')$ to $u(\alpha)$ along a surface of constant ψ,

$$u(\alpha)=\pm\sqrt{[u'(\alpha')]^2+\frac{\cos\alpha-\cos\alpha'}{2}}. \tag{9}$$

In particular, the mapping for $\alpha=0$ is given by

$$u|_{\alpha=0} = \pm\sqrt{\frac{1-\cos\alpha'+2u'^2}{2}}. \tag{10}$$

Consider the normalized current density profile along a cut through the widest part of the magnetic island ($\alpha'=0$),

$$K(u',\alpha'=0) \equiv \mu_0 J^{0\zeta}/B^{0\zeta}|_{(u',\alpha'=0)} = \begin{cases} K_0 + K_1(-1-u') & u' < -1 \\ K_0 & |u'| \leq 1 \\ K_0 + K_1(1-u') & u' > 1 \end{cases} \tag{11}$$

where K_0 and K_1 are constants determined by the local current density profile near the island. The normalized current density at any point along each magnetic surface is then given by

$$K(u,\alpha) = K(u',\alpha'=0) \tag{12}$$

and the axisymmetric averaged current density is given by

$$K^0(u) \equiv \mu_0 J^{0\zeta}/B^{0\zeta}|_u = \frac{1}{2\pi}\int_{-\pi}^{\pi} K(u,\alpha)d\alpha. \tag{13}$$

When $|u|<1$, the integral along α is separated into the part of the integration path that is inside the magnetic island and the part of the path that is outside the island, as illustrated in Fig. 2. These two parts of the integration path are divided by the value of α at the separatrix

$$\alpha_s = \cos^{-1}(2u^2-1) = \pi - 2\sin^{-1}[\min(1,|u|)]. \tag{14}$$

The expression for the axisymmetric averaged normalized current density is determined by Eqs. (9), (11), and (13) to obtain

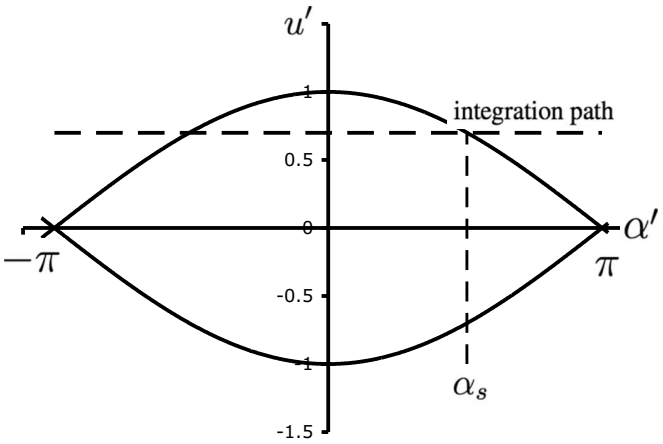

FIG. 2. Sketch of integration path for $u<1$.

$$K^0(u) = \begin{cases} K_0 + \dfrac{K_1}{\pi}\left[-\alpha_s - 2\sqrt{1+u^2}E\left(\phi_m, \dfrac{1}{1+u^2}\right)\right] & u>0 \\ K_0 + \dfrac{K_1}{\pi}\left[\alpha_s - 2\sqrt{1+u^2}E\left(\phi_m, \dfrac{1}{1+u^2}\right)\right] & u<0 \end{cases} \tag{15}$$

where

$$\phi_m = \sin^{-1}[\min(1,|u|)] \tag{16}$$

and $E(\phi,m)$ is the incomplete elliptic integral of the second kind. [Note that in Ref. 14 the notation $\mathrm{E}(\phi,k)$ is used, where $k^2 \equiv m$.] The radial derivative of the axisymmetric normalized average current density is found to be

$$\frac{d}{dV}\frac{\mu_0 J^{0\zeta}}{B^{0\zeta}} = \frac{dK^0}{dV} = -\frac{K_1}{\pi H_{mn}}\left\{\frac{2}{\sqrt{1-u^2}} - \frac{2|u|}{\sqrt{1+u^2}}E\left(\phi_m, \frac{1}{1+u^2}\right) - \frac{2}{\sqrt{1-u^2}} + \frac{2|u|}{\sqrt{1+u^2}}\left[E\left(\phi_m, \frac{1}{1+u^2}\right) - F\left(\phi_m, \frac{1}{1+u^2}\right)\right]\right\}$$
$$= \frac{2K_1}{\pi H_{mn}}\frac{|u|}{\sqrt{1+u^2}}F\left(\phi_m, \frac{1}{1+u^2}\right), \tag{17}$$

where $F(\phi,m)$ is the incomplete elliptic integral of the first kind. This result is used in Eq. (6), which is then integrated to compute the saturated magnetic island widths.

III. EFFECT OF CURRENT DRIVE WITH GAUSSIAN PROFILE ON NTM ISLAND WIDTH

If a localized current drive is added to the current density profile through the widest part of the island given in Eq. (11), there is an additional term for the current drive density, K_{EC}, which has components both inside and outside the island

$$\frac{\mu_0 J^{\zeta}}{B^{\zeta}} \equiv K(u) = \begin{cases} K_0 + K_1(-1-u) + K_{EC}(u) & u<-1 \\ K_0 + K_{EC}(u) & |u|<1 \\ K_0 + K_1(1-u) + K_{EC}(u) & u>1. \end{cases} \tag{18}$$

Here, the driven current density profile K_{EC} is assumed to have a Gaussian form, as shown in Fig. 3,

$$K_{EC}(u) = K_m \exp\left[\frac{-(u-a)^2}{2\sigma^2}\right], \tag{19}$$

where a is the offset, K_m is the maximum height, and σ is the variance.

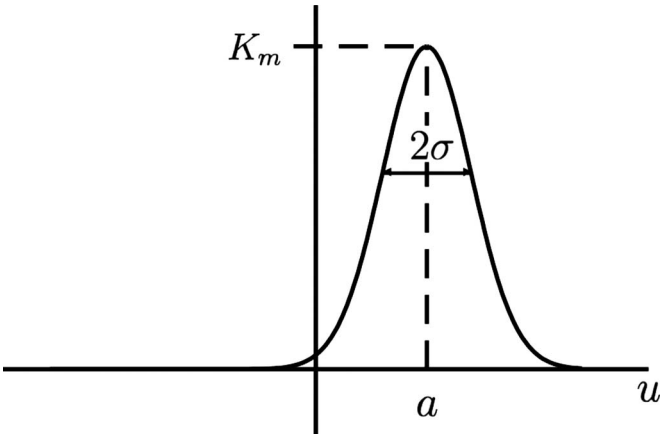

FIG. 3. Sketch of current density $K_{EC}(u)$, where K_m is the maximum height, a is the offset, and σ is the variance.

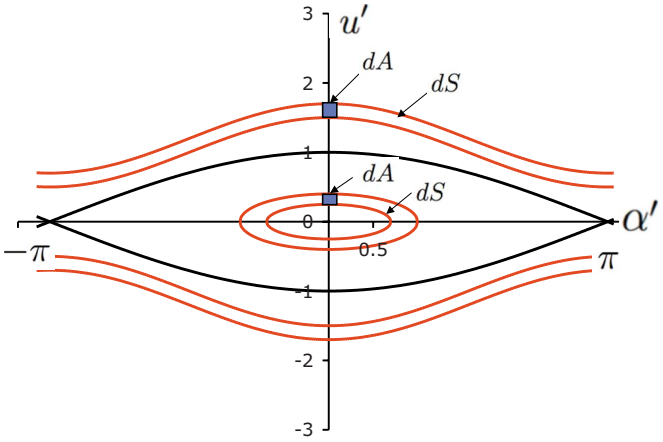

FIG. 4. (Color online) Shape of magnetic flux surfaces.

Since the terms in the current density profile, Eq. (18), are linear and since the first two terms in Eq. (18) are the same as those in Eq. (11), it is possible to consider the current drive term separately because all the other terms will not be affected. Note that the height, width, and offset of the current drive are free parameters in Eq. (19). For a centered Gaussian with a width on the order of the island width, this current drive shape is qualitatively similar to the centered parabolic current peaking factor introduced in Ref. 14. Thus, the results for the Gaussian shape can be compared with results from the parabolic peaking factor model in the case of centered current drives.

Although the current drive is located at helical angle α, the current spreads over the surface of constant ψ. When the mapping given in Eq. (9) is used in Eq. (19), the current density that results is given by

$$K_{EC}(\psi) = K_m \exp\left[\frac{-1}{2\sigma^2}\left(\pm\sqrt{\frac{\cos\alpha - \cos\alpha' + 2u'^2}{2}} - a\right)^2\right]\left(\frac{dA}{dS}\right). \tag{20}$$

The factor dA/dS results from the fact that the current applied to an area dA in u-coordinates is spread over an area dS in ψ-coordinates, as illustrated in Fig. 4, where the shapes of surfaces of constant magnetic flux ψ are shown according to Eq. (7). In this expression, the angle α represents the current drive location and α' represents the angle over which the current density is spread. Note that current can be driven over any range of helical angle α. In Sec. IV A, it will be assumed that modulated current is driven only at $\alpha=0$. The current density given by Eq. (20) is plotted in Fig. 5. For the plots in Fig. 5, $\alpha=0$, $\sigma=0.2$, $dA/dS=1$, and an arbitrary choice is made for K_m, the peak value.

In the investigation of the effects of current drive on NTMs, it is necessary to carry out the integration of Eq. (20) over both α and α' in order to determine the axisymmetric averaged current drive density. Then the derivative of averaged current drive density is added to the derivative of the background current density in order to calculate the $d(\mu_0 J^{0\zeta}/B^{0\zeta})/dV$ term required in Eq. (6). This result is then used in the ISLAND module to determine the widths of the islands.

Direct integration of the current drive profile, Eq. (20), produces the expression

$$K_{EC}^0 = \frac{1}{\pi}\int_0^{\pi}\int_{\alpha}^{\pi} K_{EC}(\psi)d\alpha' d\alpha = \frac{K_m}{\pi}\left\{\int_0^{\alpha_s}\int_{\alpha}^{\alpha_s} \exp\left[\frac{-1}{2\sigma^2}\left(\pm\sqrt{\frac{\cos\alpha - \cos\alpha' + 2u'^2}{2}} - a\right)^2\right]\left(\frac{dA}{dS}\right)_{\text{in}} d\alpha' d\alpha \right.$$
$$\left. + \int_{\alpha_s}^{\pi}\int_{\alpha}^{\pi} \exp\left[\frac{-1}{2\sigma^2}\left(\pm\sqrt{\frac{\cos\alpha - \cos\alpha' + 2u'^2}{2}} - a\right)^2\right]\left(\frac{dA}{dS}\right)_{\text{out}} d\alpha' d\alpha\right\}, \tag{21}$$

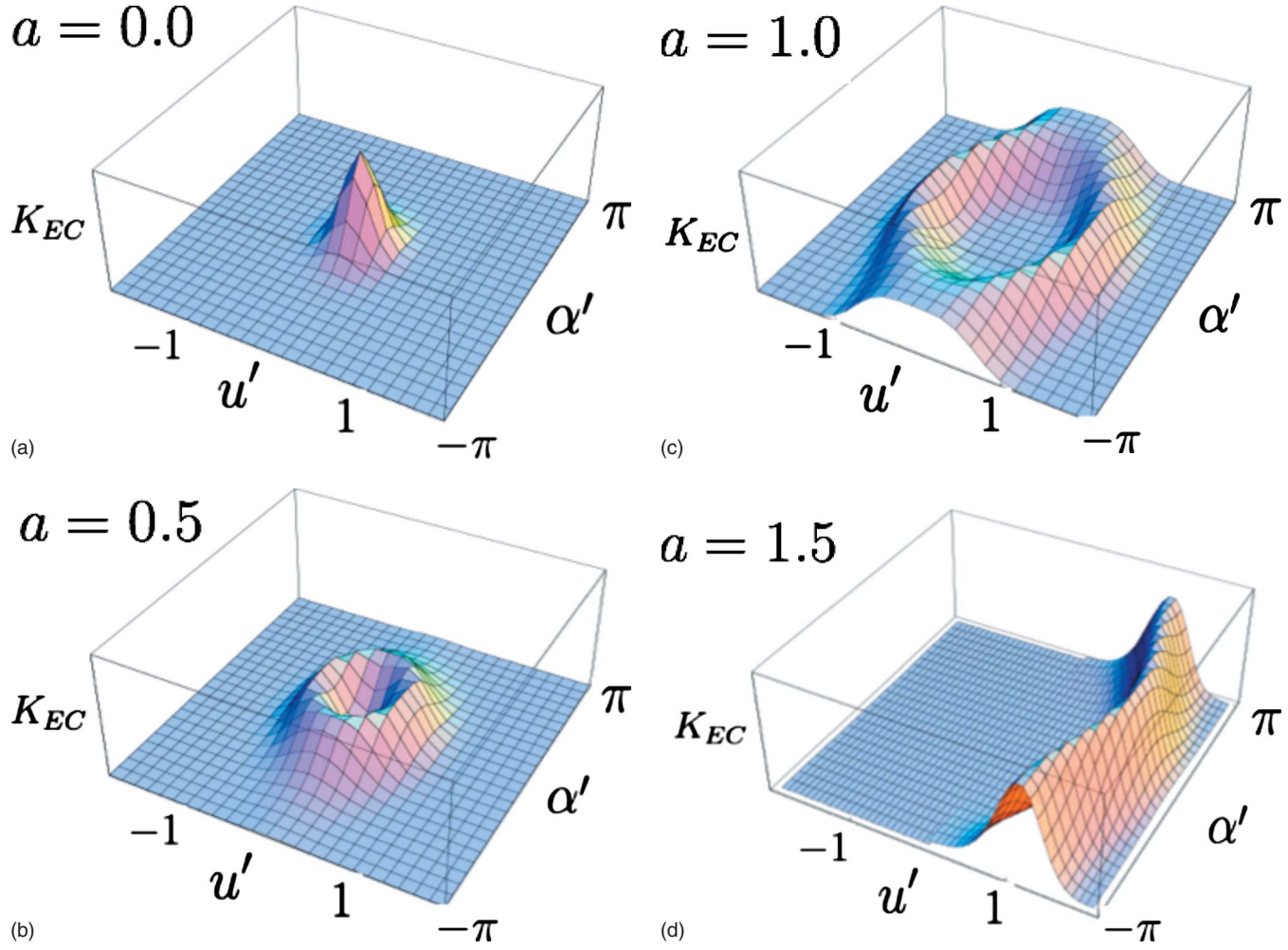

FIG. 5. (Color online) Current density after spreading over flux surfaces for various offsets.

where the separatrix value α_s is defined in Eq. (14), and $(dA/dS)_{\text{in}}$ and $(dA/dS)_{\text{out}}$ are the ratios of the area of the current drive relative to the area over which the current density spreads inside and outside the island. These differential area ratios will be discussed in detail in Sec. V. Even if dA/dS were taken to be constant, the integrals of Eq. (21) cannot be carried out analytically.

IV. MODULATED CURRENT DRIVE IN CONTRAST TO CONTINUOUS CURRENT DRIVE

As the magnetic islands rotate about the tokamak, it is possible either to modulate the current drive, ideally depositing current directly at the islands' "O-point" center, or to leave the current drive on steadily resulting in continuous current drive. The somewhat idealized case of current driven entirely at the O-point, which results in a simplification of the integral equation (21), will be considered Sec. IV A, and continuous current drive, which is experimentally more straightforward, will be considered in Sec. IV B.

A. Modulated current driven at the O-point

The integral in Eq. (21) is complicated because the effects of current spreading over flux surfaces (corresponding to the α' integral) and the effect of island rotation (which spreads the current drive over angle α for a given value of u). Both of these effects are taken into consideration in the following derivation.

In this section, a modulated current drive scenario is considered in which the current is driven only near the widest part of the island, near $\alpha=0$. This approximation makes it possible to set $\cos\alpha=1$ in Eq. (21), leaving only the single integral over α',

$$K_{EC}^{0}=\frac{K_m}{\pi}\left\{\int_0^{\alpha_s}\exp\left[\frac{-1}{2\sigma^2}\left(\pm\sqrt{\frac{1-\cos\alpha'+2u^2}{2}}-a\right)^2\right]\left(\frac{dA}{dS}\right)_{in}d\alpha'\right.$$
$$\left.+\int_{\alpha_s}^{\pi}\exp\left[\frac{-1}{2\sigma^2}\left(\pm\sqrt{\frac{1-\cos\alpha'+2u^2}{2}}-a\right)^2\right]\left(\frac{dA}{dS}\right)_{\text{out}}d\alpha'\right\}, \tag{22}$$

where the prime on the u' of Eq. (21) has been dropped. The integrals in Eq. (22) are computed numerically using a trapezoidal rule. When performing this integration, it is important to note that inside the island (corresponding to the integration from 0 to α_s), the results will be symmetric in u. Mathematically, this requires taking half the sum of the integrals along positive u, corresponding to the (+) sign in Eq. (22), and the integral along negative u, corresponding to the (−) sign. Outside the island, the upper (+) sign of Eq. (22) is used for the outboard island edge and the lower (−) sign is used for the inboard edge.

B. Continuous current drive

While current drive that is modulated with a peak at the island O-point is expected to be the most effective technique for shrinking saturated magnetic island widths, it is also useful to consider continuous current drive. Experimentally, it is often easier to implement continuously driven current since magnetic islands rotate helically about the tokamak, making their location difficult to determine in real time.

Continuously driven current is implemented by using the general double integral of Eq. (21), without setting $\alpha=0$ as in the previous subsection. This double integral is performed numerically by using the trapezoid rule twice. The discussion of the previous subsection for the sign choice in Eq. (21) for the outboard (+) and inboard (−) island edges still applies.

V. NORMALIZATION OF DIFFERENTIAL FLUX SURFACE AREAS

A method is presented in this section for calculating the differential area term, dA/dS in the integrals in Eq. (22) for modulated current drive and in Eq. (21) for continuous drive. An approximation is used for the calculation of the differential area based on the idea that the Gaussian current profile has a maximum at a, where it is centered and a characteristic width, given by the variance σ. The magnitude of the current drive is negligible outside of a width of approximately 2σ. Therefore, in this approximation, the differential area in which the current is driven is computed only in a rectangle of area

$$dA=2\sigma\times 2\delta\alpha, \tag{23}$$

where $2\delta\alpha$ is the angular coordinate extent of the current drive, as shown in Fig. 6.

The current drive that is applied in differential area dA is spread over the region between flux surfaces with area dS. Any part of the differential flux surface area dS that is inside the island can be approximated by the area between two ellipses whose semiminor axes differ by 2σ, where σ is the variance of the Gaussian current drive. The notation a_1 is used for the semiminor axis of the smaller ellipse and a_2 for the semiminor axis of larger ellipse, where $a=(a_1+a_2)/2$ is the offset of the current drive. Similarly, b_1 and b_2 denote the semimajor axis of the smaller and larger ellipses. It is assumed that all the ellipses have the same elongation π, found from the ratio of the angular length of the island ($=2\pi$) to the normalized width of the island at its widest point ($=2$), so that

$$\frac{b}{a}\approx\frac{b_1}{a_1}\approx\frac{b_2}{a_2}\approx\pi. \tag{24}$$

The differential area between flux surfaces inside an island is then given by

$$dS_{\text{in}}=\pi(a_2b_2-a_1b_1)=\pi^2(a_2^2-a_1^2)$$
$$=\pi^2[(a_2-a_1)(a_2+a_1)]=\pi^2[(2\sigma)(2a)]=4\pi^2\sigma|a|, \tag{25}$$

where the absolute value $|a|$ is used since the normalization is independent of the sign of a, and the area element is always positive. Equations (23) and (25) lead to the approximate result

$$\left(\frac{dA}{dS}\right)_{\text{in}}\approx\frac{\delta\alpha}{\pi^2|a}} \tag{26}$$

for $|a|>\sigma$. A simple way to generalize this result to include $|a|<\sigma$ is to use

$$\left(\frac{dA}{dS}\right)_{\text{in}}\approx\frac{\delta\alpha}{\pi^2\text{Max}[|a|,\sigma]}. \tag{27}$$

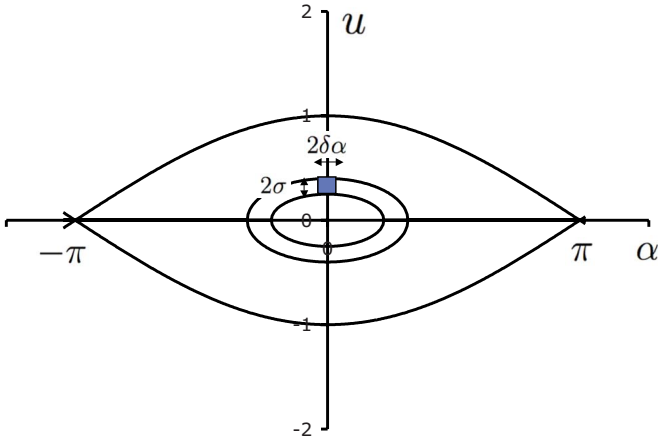

FIG. 6. (Color online) Approximation for determining dA/dS.

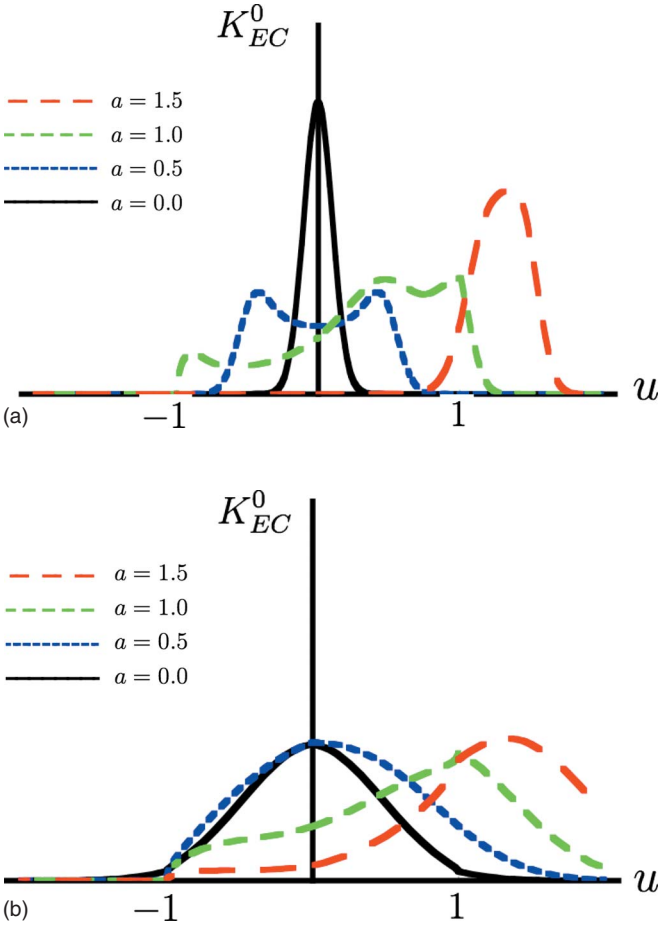

FIG. 7. (Color online) Normalization for dA/dS: (a) $\sigma=0.1$, $\delta\alpha=0.1$; (b) $\sigma=0.5$, $\delta\alpha=0.1$. The same (arbitrary) peak value and scale are used.

Far outside of the island, it is assumed that magnetic field lines are approximately straight, so that $dS_{\text{out}}=2\sigma(2\pi)$. This leads to the approximation

$$\left(\frac{dA}{dS}\right)_{\text{out}} \approx \frac{\delta\alpha}{\pi}. \tag{28}$$

However, near the island edge, dS_{out} is somewhat larger because of the curvature of the magnetic field lines. To make the differential area continuous at $|a|=1$, the following approximation is used:

$$\left(\frac{dA}{dS}\right)_{\text{out}} = \frac{\delta\alpha}{\pi^2}. \tag{29}$$

Based on these approximations for the differential area, the results for the axisymmetric averaged current drive, K^0_{EC} in arbitrary units, are shown in Fig. 7 for modulated current drives with $\delta\alpha=0.1$ and both $\sigma=0.1$ and $\sigma=0.5$. For continuous current drive, the angular width is taken to be $\delta\alpha=\pi$. It is found that more rigorous approximations to dA/dS do not significantly change the results shown in Fig. 7 and, consequently, they have not been implemented in the revised ISLAND module.

With any choice of approximation for dA/dS, an important check is to determine whether total current is conserved. The total current applied I_{tot} is proportional to I, where

TABLE I. Total current integrals for $\delta\alpha=0.1$, $\sigma=0.1$, $K_m=3.99$.

Offset	$a=0$	$a=0.5$	$a=1$	$a=1.5$
I	0.051	0.069	0.102	0.074

$$I = \delta\alpha \int_{-\infty}^{\infty} K_{EC} du. \tag{30}$$

For I to be conserved,

$$\delta\alpha \int_{-\infty}^{\infty} K_{EC} du = \int_{-\infty}^{\infty} \int_{-\pi}^{\pi} K_{EC}(\psi) d\alpha du$$

$$= 2\pi \int_{-\infty}^{\infty} K^0_{EC}(u) du. \tag{31}$$

The results for the right-hand side of Eq. (31) are presented in Table I for modulated current drive with $\delta\alpha=0.1$, $\sigma=0.1$, and the peak Gaussian value $K_m=1/(\sigma\sqrt{2\pi})=3.99$. Since the original Gaussian current drive is normalized, the left-hand side of Eq. (31) is equal to $\delta\alpha=0.1$. From the results in Table I, it can be seen that current is not conserved when the approximation described above is applied. This discrepancy has to do with the approximations made in both cases, namely, the assumption that all the closed flux surfaces are ellipses and flux surfaces outside islands are straight lines. These approximations do not hold near the island edge. Further, the approximations were made for current driven near the island center. These approximations lead to discrepancies of up to a factor of 2 from the expected value in Table I. However, it is possible to adjust for the approximations and to ensure that the total current is in fact conserved, by applying a renormalization factor (simply a constant). This renormalization is implemented in the revised ISLAND module.

VI. COMPUTING THE TOTAL DRIVEN CURRENT IN AMPERES

A. Conversion to real, physical units

In practice, the physical current drive parameters (offset a_{real}, width σ_{real}, and magnitude $K_{m,\text{real}}$) are given in units of length (m) and current density (A/m^2). Therefore, it is necessary to convert from the real, physically relevant units to the more convenient normalized units used in previous subsections. As defined previously, a and σ are dimensionless variables normalized by the magnetic island half-width H_{mn} in meters,

$$a = a_{\text{real}}/H_{mn} \quad \text{and} \quad \sigma = \sigma_{\text{real}}/H_{mn}. \tag{32}$$

For the current density peak K_m, the conversion depends on the total plasma input current. Since the NTCC ISLAND module comes with two test input files, input_JET and input_DIIID,[12] only these will be considered here. The units of K_m as used by the code are $1/\text{m}$. This is equivalent to the current peaking factor in Ref. 14. This current peaking factor and K_m have units of $\mu_0 J/B$, where J and B are the toroidal current density and magnetic field, respectively. Since, for a given input, the magnetic field is constant, $K_{m,\text{real}}$ in A/m^2 is

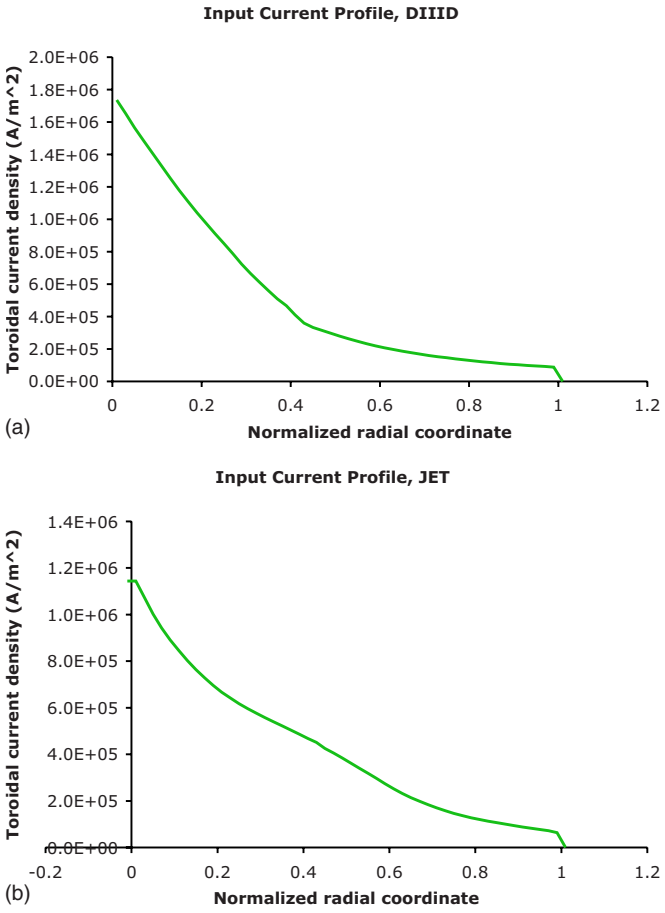

FIG. 8. (Color online) Sample input current profiles.

converted to K_m using the average input current. The input current profiles are shown in Fig. 8, and the conversion is summarized in Table II.

B. Current peaking factor method: Applied current

It is of interest to compare results obtained by the procedure outlined in this paper to those obtained from the implementation of the simple parabolic current peaking factor presented in Ref. 14, where the current density profile through the widest part of the island is given by

$$K_C = C(1-u^2)\delta(\alpha). \tag{33}$$

Here, $\delta(\alpha)$ is the Dirac delta function and C is the current peaking factor. (Note, C has units of 1/rad, $K=\mu_0 J/B$, has units of 1/rad, and J has units of A/m rad.) To convert to physical units of (A/m rad), multiply by $1/\mu_0 B$, i.e.,

TABLE II. Conversion of K_m to real units.

	K_m	$K_{m,\mathrm{real}}$
JET	1 (1/m)	2.336×10^6 (A/m^2)
DIIID	1 (1/m)	1.592×10^6 (A/m^2)

$$K_{C,\mathrm{real}} = C(1-u^2)\delta(\alpha)\left(\frac{1}{\mu_0 B}\right). \tag{34}$$

The total current in Amperes is then found by integrating over u (the normalized radial coordinate) and α (the normalized angular coordinate) and multiplying by the half-width H_{mn},

$$I_{\mathrm{tot}} = H_{mn}C\left(\frac{1}{\mu_0 B}\right)\int_{-\infty}^{\infty}\int_{-\infty}^{\infty}(1-u^2)\delta(\alpha)dud\alpha$$

$$= H_{mn}C\left(\frac{1}{\mu_0 B}\right)\int_{-\infty}^{\infty}(1-u^2)du. \tag{35}$$

C. Gaussian current drive: Applied current

The current drive in the ISLAND module code is given by Eq. (19). The units of K_{EC} are 1/rad, as are the units of K_C. To convert to real units for the applied current drive density, it is necessary to multiply by $1/\mu_0 B$,

$$K_{EC,\mathrm{real}} = K_m \exp\left[\frac{-(u-a)^2}{2\sigma^2}\right]\left(\frac{1}{\mu_0 B}\right). \tag{36}$$

In order to calculate the total current in Amperes, this expression is integrated over u and α and multiplied by the half-width H_{mn}. The integral over α is just a constant $\delta\alpha$, since the driven current is applied over this small angular region. The result is

$$I_{\mathrm{tot}} = H_{mn}\delta\alpha K_m\left(\frac{1}{\mu_0 B}\right)\int_{-\infty}^{\infty}\exp\left[\frac{-(u-a)^2}{2\sigma^2}\right]du. \tag{37}$$

D. Current after spreading: Current peaking factor

After the current is spread over flux surfaces, the average current drive is given by the integral

$$K^0 = \frac{1}{2\pi}\int_{-\pi}^{\pi}K(\psi)d\alpha. \tag{38}$$

For the parabolic current peaking factor method, the current density and the total current are given by

$$K_C(\psi) = C[1-u^2(\psi)], \tag{39}$$

$$K_{C,\mathrm{real}}(\psi) = C\left(\frac{1}{\mu_0 B}\right)[1-u^2(\psi)], \tag{40}$$

$$I_{\mathrm{tot}} = H_{mn}C\left(\frac{1}{\mu_0 B}\right)\int_{-\pi}^{\pi}\int_{-\infty}^{\infty}[1-u^2(\psi)]dud\alpha$$

$$= \frac{2\pi H_{mn}}{\mu_0 B}\int_{-\infty}^{\infty}K_C^0 du. \tag{41}$$

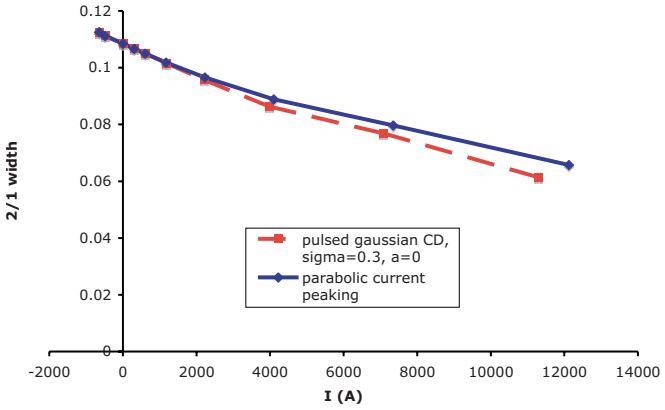

FIG. 9. (Color online) Saturated island width as a function of total driven current for parabolic current peaking factor (solid) and modulated Gaussian current drive with $\sigma=0.3$ and $a=0$ (dashed).

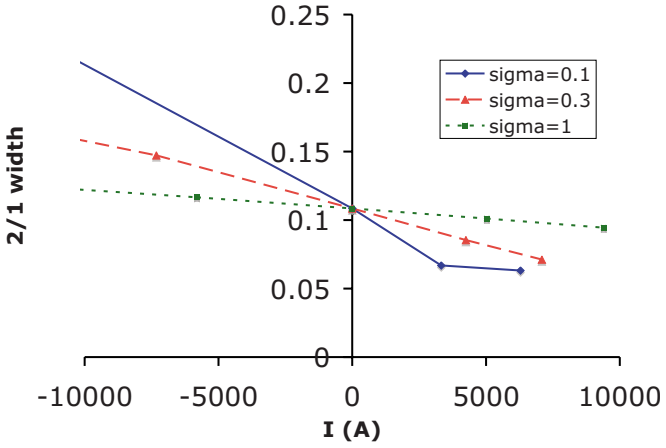

FIG. 10. (Color online) Saturated island width as a function of total driven current for centered, modulated Gaussian current drive with different widths.

E. Current after spreading: Gaussian

In a similar manner, for the Gaussian current drive, the current density and total current are given by

$$K_{EC}(\psi) = K_m \exp\left\{\frac{-[u(\psi)-a]^2}{2\sigma^2}\right\}, \tag{42}$$

$$K_{EC,\mathrm{real}}(\psi) = K_m\left(\frac{1}{\mu_0 B}\right)\exp\left\{\frac{-[u(\psi)-a]^2}{2\sigma^2}\right\}, \tag{43}$$

$$I_{\mathrm{tot}} = H_{mn}K_m\left(\frac{1}{\mu_0 B}\right)\int_{-\pi}^{\pi}\int_{-\infty}^{\infty}\exp\left\{\frac{-[u(\psi)-a]^2}{2\sigma^2}\right\}dud\alpha$$

$$= \frac{2\pi H_{mn}}{\mu_0 B}\int_{-\infty}^{\infty}K_{EC}^0 du. \tag{44}$$

VII. REVISED ISLAND MODULE RESULTS

A. Results for modulated current drive

Results are presented in Figs. 9–12 for the change in the island width produced by current drive computed using the revised ISLAND module. These results are for $m/n=2/1$ islands only. In each plot, the island width is normalized by the plasma minor radius.

In Fig. 9, the island width is shown as a function of driven current for a centered modulated Gaussian current drive profile with $\sigma=0.3$, $a=0$ (dashed curve). For comparison, results are shown using the simple parabolic current peaking factor as well (solid curve). The maximum driven current in Fig. 9 corresponds to about 20% of the total background plasma current. In both cases, higher levels of total driven current shrink the island to lower saturated widths. The curves for the modulated Gaussian and the parabolic current drive profiles are similar, as is to be expected for a centered Gaussian with a width comparable to the parabolic current peaking factor within the island. A slight leveling off of the island width for large current drive is also illustrated in Fig. 9. The neoclassical tearing mode is linearly stable, which means that below a certain critical width, magnetic islands will continue to shrink on their own. The ISLAND module is not valid for these small island widths, which helps to explain the leveling of the curves in Fig. 9.

Figure 10 illustrates the effect of changing the width of the centered modulated Gaussian current drive with zero offset or, equivalently, changing the variance of the Gaussian, σ, while fixing the offset at $a=0$. It can be seen that a narrow current drive (small σ) is more effective at shrinking the island than a broader current drive (the slope of the $\sigma=0.1$ curve is more negative than the slope of the $\sigma=0.3$ and $\sigma=1.0$ curves in Fig. 10). For current driven with a broad width (such as $\sigma=1$), much of the driven current falls outside the island, Since the portion of current driven outside of the island can have a destabilizing effect, it competes with the stabilizing effect associated with the fraction of the current driven inside the island.

Figure 11 shows the effect of changing the offset of the current drive center relative to the island center. Results are shown for different magnitudes of driven current. Here the width of the Gaussian is fixed at $\sigma=0.4$, and the offset a is

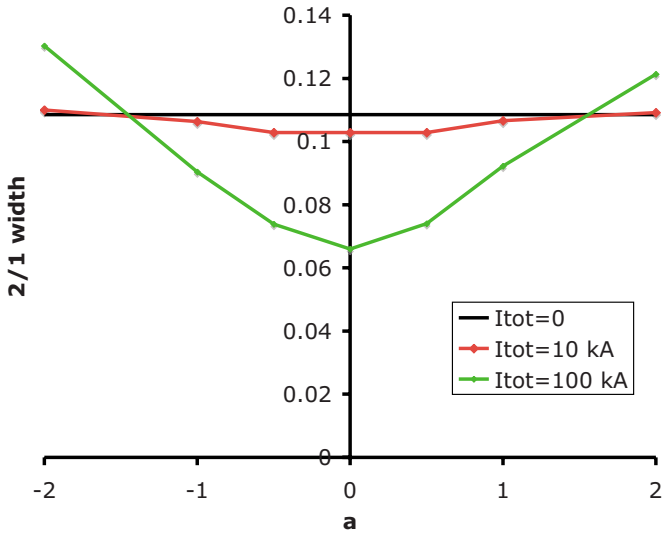

FIG. 11. (Color online) Saturated island width as a function of offset for modulated Gaussian current drive with various (approximate) total current drive levels.

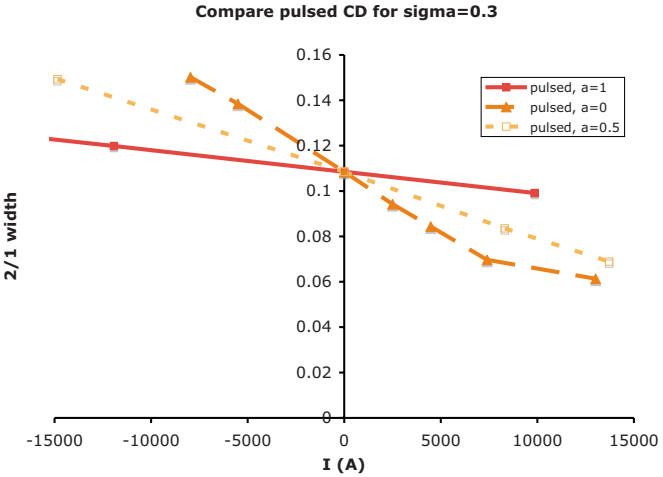

FIG. 12. (Color online) Saturated island width as a function of driven current for modulated Gaussian current drive with $\sigma=0.3$ with three different offsets.

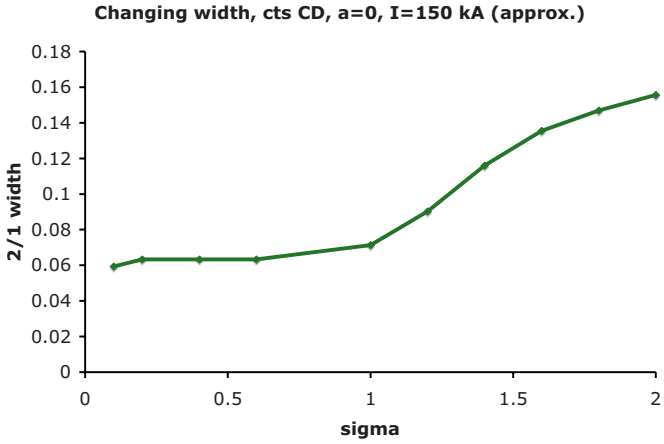

FIG. 14. (Color online) Dependence of saturated island width on the width, σ, of the with continuous Gaussian current drive for $a=0$ and $I_{tot}\approx 1.5\times 10^5$ A.

varied. A centered current drive is most effective at shrinking the island, while a sufficiently off-center current drive eventually becomes destabilizing. The destabilizing effect is greater for current driven on the inboard side of the island (for negative a) than on the outboard side (positive a). The island width is plotted as a function of the magnitude of the modulated current drive for a selection of different offsets in Fig. 12. As expected, the slope of the saturated island width curve is most negative for centered ($a=0$) drive, and flat test for $a=1$.

B. Results for continuous current drive

Qualitatively, the results obtained when continuous current drive is applied are similar to those presented in the previous subsection for modulated current drive. For example, in the case of zero offset current drive ($a=0$) with a width on the order of the island width ($\sigma=1$), it is found that the saturated island width shrinks as the total driven current is increased. This relationship is shown in Fig. 13. When the total driven current is held constant, along with zero offset ($a=0$), a narrower current drive profile is expected to be more effective in shrinking the islands than a broad current drive profile. This behavior is found, although the relationship is not linear, as shown in Fig. 14.

For a constant level of driven current, where both the peak K_m and the width σ are held fixed, a centered current drive ($a=0$) is most effective at shrinking the islands. This is shown for different levels of total continuously driven current in Fig. 15. It can also be seen in Fig. 15 that outboard current drive (positive a) is more stabilizing than an inboard current drive, as has been noted in the previous section. Also, for large offsets, a continuous current drive is destabilizing, as it was for a modulated current drive.

In Fig. 16, the island width is plotted as a function of the magnitude of the continuously driven current for a selection of various offsets. The corresponding plot for modulated current is shown in Fig. 12. Again, the slope of the curve is most negative for centered ($a=0$) Gaussian current drive, indicating that centered current drive profile is most stabilizing. When the offset of the continuous current drive is on the

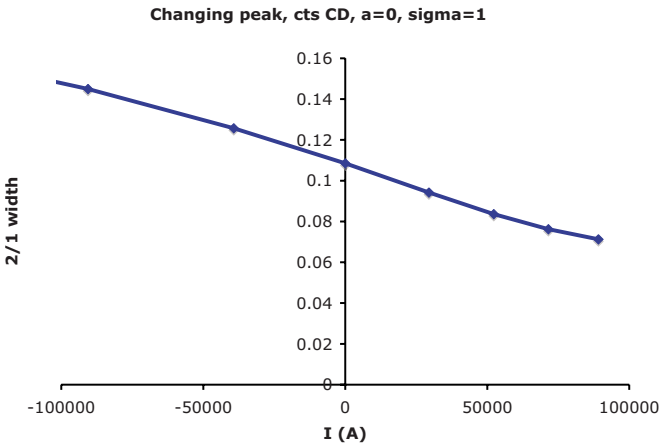

FIG. 13. (Color online) Saturated island width as a function of total drive current for continuous Gaussian current drive with $a=0$, $\sigma=1$. The range is about 20% of the background current.

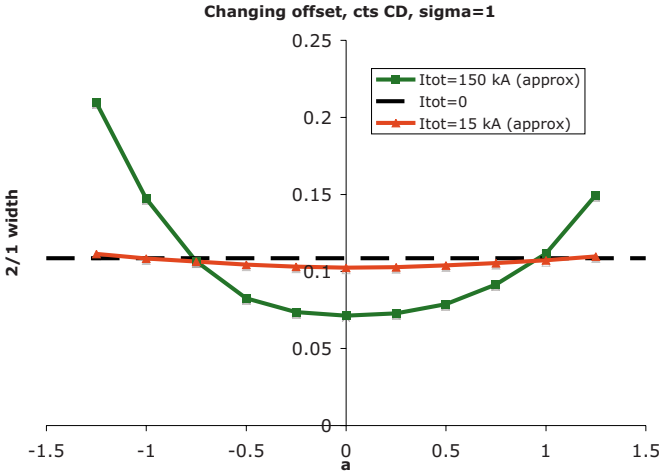

FIG. 15. (Color online) Illustration of the dependence of saturated island width on offset a for continuous Gaussian current drive with $\sigma=1$. Results are shown for three values of I_{tot}.

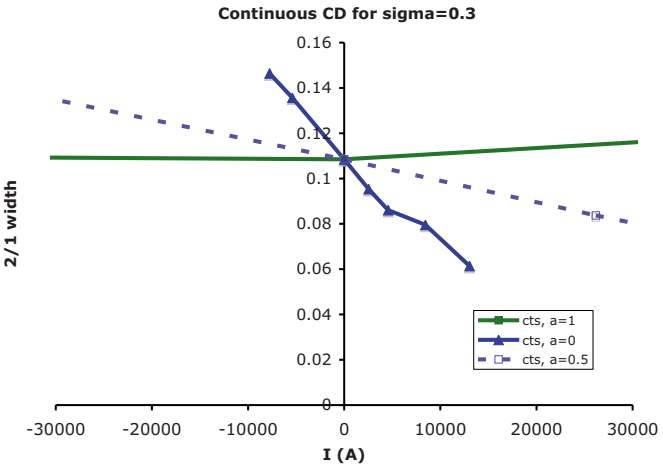

FIG. 16. (Color online) Saturated island as a function of total current drive for continuous Gaussian current drive.

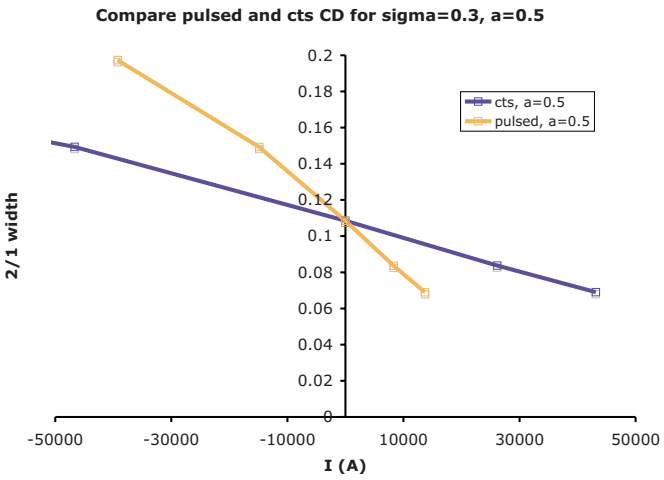

FIG. 18. (Color online) Saturated island width as a function of the total driven current for modulated and continuous Gaussian current that is driven off axis (a=0.5, σ=0.3).

order of the island width, a positive continuous current drive becomes destabilizing, as indicated by the positive slope of the a=1 curve in the positive current region of Fig. 16.

C. Comparing effects of modulated and continuous current drive

The previous two subsections provide illustrations of many of the qualitative similarities between current drive that is modulated at the angle of the island O-point and current drive that is on continuously. More quantitative comparisons are presented in this subsection in order to illustrate which type of current drive profile is more efficient at shrinking the islands. In particular, for a given amount of total current, is it better to pulse the current drive entirely at the angle of the island O-point, or to leave the current on continuously as the islands rotate about the tokamak? It is important to understand how different are the results.

The saturated island width computed using the revised ISLAND module is plotted as a function of the driven current in Fig. 17 for a case with centered modulated Gaussian current drive and a comparable case with centered continuous Gaussian current drive. Also shown in this figure are results for the island width for the original parabolic current peaking factor. The case of the parabolic peaking factor corresponds to an example of a modulated current that is driven entirely within the island. As shown before, this modulated parabolic current drive is quite similar to the centered modulated Gaussian current drive. It can be seen in Fig. 17 that the effect of a continuous Gaussian current drive is nearly the same as the effect of a modulated Gaussian current drive when both current drive profiles are centered and relatively narrow.

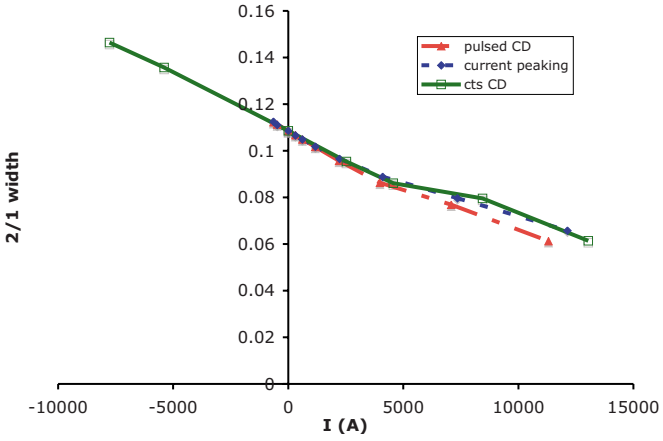

FIG. 17. (Color online) Saturated island width as a function of the total driven current centered at the mode rational surface. Results are obtained for a parabolic current drive profile, for a Gaussian current drive profile that is modulated (a=0, σ=0.3), and for a continuous Gaussian current drive profile (a=0, σ=0.3).

Results are shown in Fig. 18 for a Gaussian current drive that is offset from the island center by half the island width, a=0.5, using the same width σ=0.3 as in Fig. 17. Now the results are very different for modulated and continuous current drives. It can be seen that the modulated current drive is much more effective at shrinking the island for this case, as the slope of the corresponding curve is more negative. Increasing the offset of both the modulated and continuous current drive to the outboard edge of the island (a=1) exaggerates this effect further, as shown in Fig. 19. Here, for the same Gaussian width, σ=0.3, the modulated current drive stabilizes the magnetic island for positive current while the continuous drive is destabilizing.

VIII. CONCLUSIONS

A model for using localized current drive to stabilize a neoclassical tearing mode instability has been developed and implemented in the revised ISLAND module for both modulated and continuous current drive (driven at the angle of the island O-point). For both modulated and continuous current drive, it was shown that, when the current drive is radially centered on the island, narrow current drive profiles are more efficient at shrinking the magnetic islands than wide current drive profiles, for which a significant component of the driven current is located outside the island. It was also illustrated that, when the current drive width is held fixed, current drive profiles that are radially centered at the island center

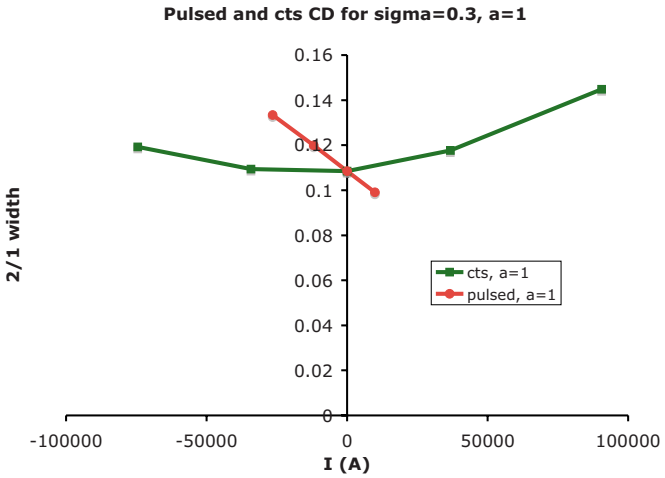

FIG. 19. (Color online) Saturated island width as a function of the total driven current for modulated and continuous current drive with $a=1$ and $\sigma=0.3$. In this instance, the driven current is centered at the outboard edge of the island.

shrink the islands more efficiently than current drive profiles that are offset from the island center. For current drive offsets from the island center that are sufficiently large relative to the island width, the effect of positive current drive is destabilizing, resulting in larger island widths. For both modulated and continuous current drive, this destabilizing effect is stronger for current driven at the inboard island edge rather than the outboard edge.

When simulation results with modulated current drive are compared with results obtained in which continuous current drive is applied, it is found that the modulated current drive is more effective at shrinking the island for equal amounts of total current. This result is expected, since current modulated at the island O-point injects far more current into the island and less outside.

The study of current drive with a radial offset with respect to the island provides the foundation for future computational work on feedback stabilization of the neoclassical tearing modes. These simulation results, which are consistent with experimental results, indicate that a radially centered current drive will have the strongest stabilizing effect, represented by a local minimum on a plot of saturated magnetic island width as a function of current drive offset. This minimum lends itself particularly well to extremum seeking control,[16] for which the location of the island need not necessarily be known. Such a control algorithm could represent an improvement over current "search and suppress" algorithms.[9]

ACKNOWLEDGMENTS

This work was supported in part by a grant from the Commonwealth of Pennsylvania, Department of Community and Economic Development, through the Pennsylvania Infrastructure Technology Alliance (PITA), the NSF CAREER award program (Contract No. ECCS-0645086), and the U.S. Department of Energy under Contract No. DE-FG02-92-ER-54141.

[1] R. J. La Haye, Phys. Plasmas **13**, 055501 (2006).
[2] T. C. Hender, D. F. Howell, R. J. Buttery, O. Sauter, F. Sartori, R. J. La Haye, A. W. Hyatt, C. C. Petty, JET EFDA Contributors, and the DIII-D Team, Nucl. Fusion **44**, 788 (2004).
[3] H. Zohm, G. Gantenbein, A. Gude, S. Günter, F. Leuterer, M. Maraschek, J. Meskat, W. Suttrop, Q. Yu, ASDEX Upgrade Team, and ECRH Group (AUG), Nucl. Fusion **41**, 197 (2001).
[4] R. J. Buttery, S. Gunter, G. Giruzzi, T. C. Hender, D. Howell, G. Huysmans, R. J. La Haye, M. Maraschek, H. Reimerdes, O. Sauter, C. D. Warrick, H. R. Wilson, and H. Zohm, Plasma Phys. Controlled Fusion **42**, B61 (2000).
[5] Q. Yu, S. Günter, K. Lackner, A. Gude, and M. Maraschek, Nucl. Fusion **40**, 2031 (2000).
[6] O. Sauter, R. J. LaHaye, Z. Chang, D. A. Gates, Y. Kamada, H. Zohm, A. Bondeson, D. Boucher, J. D. Callen, M. S. Chu, T. A. Gianakon, O. Gruber, R. W. Harvey, C. C. Hegna, L. L. Lao, D. A. Monticello, F. Perkins, A. Pletzer, A. H. Reiman, M. Rosenbluth, E. J. Strait, T. S. Taylor, A. D. Turnbull, F. Waelbroeck, J. C. Wesley, H. R. Wilson, and R. Yoshinof, Phys. Plasmas **4**, 1654 (1997).
[7] C. C. Hegna and J. D. Callen, Phys. Plasmas **4**, 2940 (1997).
[8] R. Fitzpatrick, Phys. Plasmas **2**, 825 (1995).
[9] D. A. Humphreys, J. R. Ferron, R. J. La Haye, T. C. Luce, C. C. Petty, R. Prater, and A. S. Welander, Phys. Plasmas **13**, 056113 (2006).
[10] N. Hayashi, T. Ozeki, K. Hamamatsu, and T. Takizuka, Nucl. Fusion **44**, 477 (2004).
[11] G. Giruzzi, M. Zabiego, T. A. Gianakon, X. Garbet, A. Cardinali, and S. Bernabei, Nucl. Fusion **39**, 107 (1999).
[12] F. D. Halpern, G. Bateman, A. H. Kritz, and A. Pankin, J. Plasma Phys. **72**, 1153 (2006).
[13] F. D. Halpern, G. Bateman, and A. H. Kritz, Phys. Plasmas **13**, 062510 (2006).
[14] G. Bateman and R. N. Morris, Phys. Fluids **29**, 753 (1986).
[15] C. Nguyen, G. Bateman, and A. H. Kritz, Phys. Plasmas **11**, 3460 (2004).
[16] K. Ariyur and M. Krstic, *Real-Time Optimization by Extremum Seeking Feedback* (Wiley, Hoboken, NJ, 2003).